Photoinduced Charge Separation and Charge Recombination in the [60]Fullerene−Diphenylbenzothiadiazole−Triphenylamine Triad: Role of Diphenylbenzothiadiazole as Bridge

Atula S. D. Sandanayaka,[†] Yoshiki Taguri,[‡] Yasuyuki Araki,[†] Tsutomu Ishi-i,*[,§] Shuntaro Mataka,*[,§] and Osamu Ito*[,†]

Institute of Multidisciplinary Research for Advanced Materials, Tohoku University, Katahira 2-1-1, Aoba-ku, Sendai 980-8577, Japan, Interdisciplinary Graduate School of Engineering Sciences, Kyushu University, 6-1 Kasuga-kohen, Kasuga 816-8580, Japan, and Institute for Materials Chemistry and Engineering (IMCE), Kyushu University, 6-1 Kasuga-kohen, Kasuga 816-8580, Japan

Received: July 11, 2005; In Final Form: September 27, 2005

Photoinduced electron-transfer processes of the newly synthesized [60]fullerene−diphenylbenzothiadiazole−triphenylamine (C_{60}−PBTDP−TPA) triad in polar and nonpolar solvents have been studied by using time-resolved transient absorption and fluorescence measurements from picosecond to microsecond regions. By fluorescence lifetime measurements in picosecond time regions, excitation of the charge-transfer transition of the PBTDP−TPA moiety in C_{60}−PBTDP−TPA induces energy transfer to the C_{60} moiety generating $^1C_{60}$*−PBTDP−TPA, competitively with charge separation generating $C_{60}^{\bullet-}$−PBTDP−$TPA^{\bullet+}$. From $^1C_{60}$*−PBTDP-TPA, which is generated directly and indirectly, charge separation occurs generating $C_{60}^{\bullet-}$−PBTDP−$TPA^{\bullet+}$ in polar solvents. The $C_{60}^{\bullet-}$−PBTDP−$TPA^{\bullet+}$ formed via the singlet excited states decayed within a few nanoseconds as revealed by the picosecond transient absorption spectra. In the nanosecond time region, $C_{60}^{\bullet-}$−PBTDP−$TPA^{\bullet+}$ is produced slowly, probably via $^3C_{60}$*−PBTDP−TPA. Lifetimes of such slowly generated $C_{60}^{\bullet-}$−PBTDP−$TPA^{\bullet+}$ were longer than 1 μs, which are the longest values among the C_{60}−bridge−TPA triad systems reported hitherto at room temperature. Roles of the PBTDP−TPA moiety with twisted intermolecular charge-transfer character playing as energy donor and electron donor in addition to the bridge have been disclosed.

Introduction

Photoinduced energy-transfer and electron-transfer processes are the key step for photosynthetic conversion of light energy into useful electrochemical potentials, which is imperative in a variety of technological applications.[1−3] The promise of using fullerene derivatives for the design of new photochemical molecular devices has promoted researchers to develop the ways to control photoinduced electron transfer using light or other inputs.[4−6] Fullerene (C_{60}) and its simple derivatives have been incorporated in a number of electron-donor systems to develop the future molecular photovoltaic devices, which are an area of intense current research activity.[7−12] The C_{60} has many desirable properties as electron acceptor in the photoinduced electron donor−acceptor systems with low reduction potential, associating with low reorganization energy.[10−14] Synthetic developments have further opened successful methods to readily functionalize fullerenes, incorporating a number of photoactive electron donors via bridges.[15−20] Photoexcitation of either electron-donor or C_{60} of the dyad and triad leads to a charge separation to generate the radical anion of C_{60} and the radical cation of the electron-donor observable in nanosecond time region. Thus, covalently bonded C_{60}−donor dyads and triads have been successfully used in achieving one of the key requirements for artificial photosynthesis; namely, generation of long-lived charge separated states.[8−13] The efficiencies and rates of charge-separation (CS) processes in the C_{60}-based dyads and triads can be tuned by the energies of the radical ion-pairs (RIP) of the C_{60}–donor molecules, in addition to the distances and orientations between the electron-donor and C_{60} moieties.[1−6] Furthermore, the important roles of the bridged molecules connecting electron-donors and -acceptors have been pointed out.[19,20] In our previous papers,[15,18] we reported that the bridge molecular units connecting the C_{60} moiety and the donor molecules play important roles to assist the electron migration and hole migration.

4,7-Diphenyl-2,1,3-benzothiadiazole and its derivatives, which were successfully used as bridge molecules, are known as strongly fluorescent dyes.[21,22] The absorption and emitting bands can be tuned by the aromatic substituents at the 4- and 7-positions of the benzothiadiazole core (BTD). Furthermore, the benzothiadiazole unit was used as an important spacer in semiconducting oligomers.[21,22] Recently, one of our groups has developed the benzothiadiazole dyes as functional materials such as dichroic fluorescent materials[23] and red-fluorescent two-photon-absorbing materials.[24] In addition, aromatic compounds with intramolecular charge-transfer states (ICT) are useful to examine micropolarity.[25] Some of these compounds can attain

* To whom correspondence should be addressed. (O.I.) E-mail: (O.I.) ito@tagen.tohoku.ac.jp, (T.I.) ishi-i@cm.kyushu-u.ac.jp.

[†] Institute of Multidisciplinary Research for Advanced Materials, Tohoku University.

[‡] Interdisciplinary Graduate School of Engineering Sciences, Kyushu University.

[§] Institute for Materials Chemistry and Engineering (IMCE), Kyushu University.

10.1021/jp053809c CCC: $30.25
Published on Web 11/03/2005

SCHEME 1

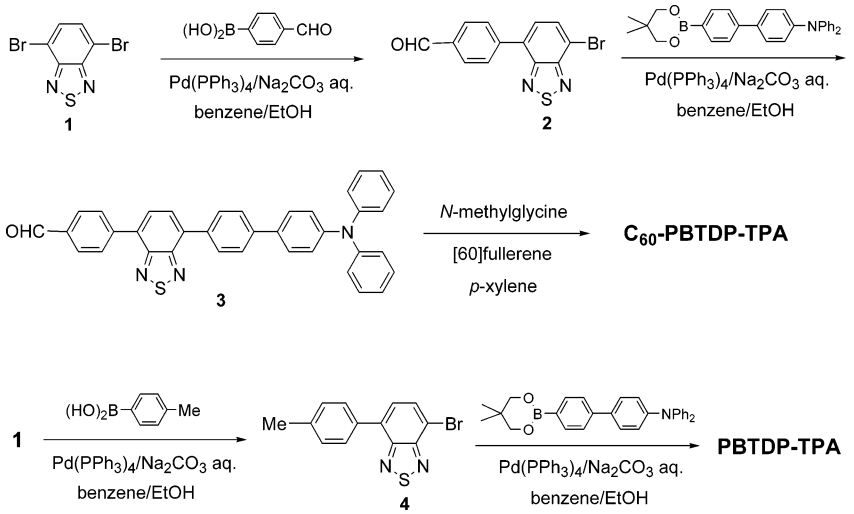

a large degree of charge-transfer by twisting about a bond that connects the donor and acceptor moieties. Recently, high efficient solar cell was constructed using benzothiadiazole core as good electron donors vs excited state of the C_{60} derivatives in the layered structure,[26] which motivated us to design the molecule covalently connected C_{60} with benzothiazole unit.

In the present study, we have prepared 4,7-diphenyl-2,1,3-benzothiadiazole (PBTDP) moiety covalently bonded to triphenylamine (TPA) used as an electron donor. Finally, C_{60} was covalently linked at one end of PBTDP−TPA as shown in Figure 1 (abbreviated as C_{60}−PBTDP−TPA). The PBTDP moiety was selected to act also as a bridge, because its excited states show the twisted intramolecular charge-transfer (TICT) behavior.[25] Comparing with our previous work;[27] the PBTDP moiety in C_{60}−PBTDP−TPA acts as weaker electronic coupled bridge with the TPA moiety, in addition to light harvesting antenna.

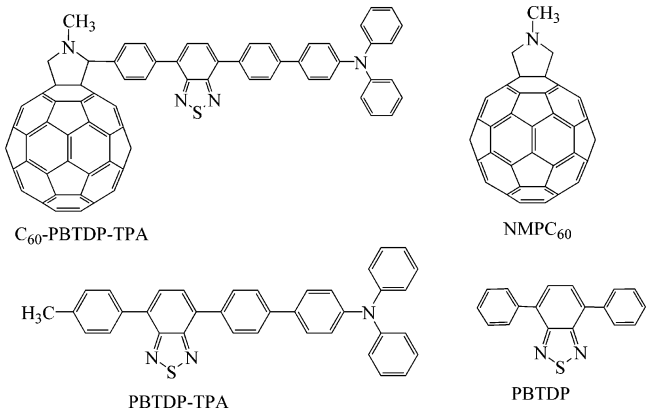

Figure 1. Molecular structures of C_{60}−PBTDP−TPA and reference compounds.

Our aim of the present study is to reveal the role of the PBTDP moiety on the efficiencies of the CS processes by probing the fluorescent states with picosecond time-resolved fluorescence measurements. The lifetimes of the CS states were measured with the picosecond and nanosecond transient spectra measurements.

Results and Discussion

Synthesis. C_{60}−PBTDP−TPA triad and its reference compound PBTDP−TPA were synthesized according to the procedures shown in Scheme 1, in which Suzuki coupling reaction and Prato reaction were used as key steps.[28] C_{60}−PBTDP−TPA and PBTDP−TPA were identified on the basis of spectroscopic methods and elemental analysis (see the Experimental Section).

Optimized Structures and Molecular Orbitals. Optimized structures calculated by the density function B3LYP/3-21G(*) method are shown in Figure 2 for C_{60}−PBTDP−TPA and PBTDP−TPA in their ground states. The center-to-center distances (R_{CC}) between the C_{60} and TPA moieties, the C_{60} and PBTDP moieties, and the PBTDP and TPA moieties were estimated to be 23.5, 11.0, and 11.5 Å, respectively. These R_{CC} values show that the center of PBTDP moiety is almost the same distance (ca. 11 Å) from the C_{60} moiety and the TPA moiety.

Figure 2 also shows the electron densities of the HOMO, LUMO, and LUMO+3 of C_{60}−PBTDP−TPA and the HOMO and LUMO for PBTDP−TPA calculated on the basis of the optimized structures. In these compounds, the majority of the electron density of the HOMO was found to be localized on the TPA moiety with a small orbital coefficient on the vicinal phenyl moiety for both C_{60}−PBTDP−TPA and PBTDP−TPA. In addition, the HOMOs for C_{60}−PBTDP−TPA and PBTDP−TPA clearly show that PBTDP moiety is not allowed to couple strongly with TPA moiety by the intermediate phenyl group. This is the prominent difference from the donors without the intermediate phenyl group as reported in our previous study.[27]

Figure 2 clearly shows that the LUMO for C_{60}−PBTDP−TPA is localized on the C_{60} spheroid. The LUMO+1 and LUMO+2, which have almost similar energy levels to that of the LUMO, are also localized on the C_{60} spheroid. On the other hand, the LUMO+3, which has higher energy than that of the LUMO, is localized on the BTD moiety similar to the LUMO of PBTDP−TPA.

Furthermore, we calculated the energy of the excited singlet states of C_{60}−PBTDP−TPA by the ZINDO(Singlets)/3-21G(*) SP method (see the Supporting Information). The energy barrier for this twisting was found to be small (0.3024 eV), supporting the TICT mechanism as a possible description of the dual fluorescence phenomenon for PBTDP−TPA.

Electrochemical Studies. The cyclic voltammogram of C_{60}−PBTDP−TPA in benzonitrile (PhCN) shows the reversible peaks in the wide region of −2.0 to +1.0 V vs Fc/Fc^+ (see the Supporting Information). From these reversible peaks, the reduction (E_{red}) and oxidation potentials (E_{ox}) of C_{60}−PBTDP−TPA were evaluated to be −1.04, −1.46, −1.88, and +0.48 V vs Fc/Fc^+ in PhCN. The first and second negative potentials

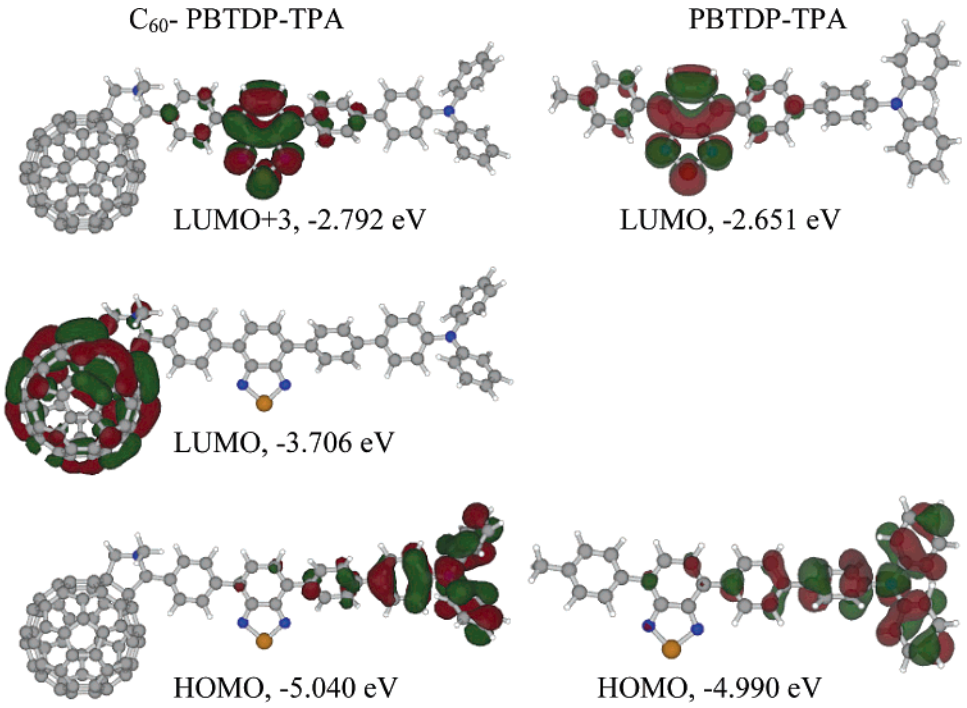

Figure 2. Frontier HOMOs and LUMOs of C_{60}−PBTDP−TPA and PBTDP−TPA calculated by density function B3LYP/3-21G(*) methods.

TABLE 1: Cyclic Voltammetry Data of C_{60}−PBTDP−TPA and PBTDP−TPA

		V vs Fc/Fc^+			
compd	solvent	E_{ox} TPA	E_{red} (C_{60})	E_{red}(C_{60})	E_{red} BTD
C_{60}−PBTDP−TPA	PhCN	0.48	−1.04	−1.46	−1.88
PBTDP−TPA	PhCN	0.48			−1.88
C_{60}−PBTDP−TPA	DMF	0.52	−0.93	−1.36	−1.77
PBTDP−TPA	DMF	0.53			−1.77

are attributed to the E_{red} values of the C_{60} moiety, the third negative potential is attributed to the E_{red} value of the PBTDP moiety, and the positive potential is assigned to the E_{ox} value of the TPA moiety in C_{60}−PBTDP−TPA by comparison with the E_{red} and E_{ox} values of reference compounds as listed in Table 1. The electrochemical investigations confirmed that there is no appreciable electronic interaction among the C_{60}, PBTDP, and TPA moieties in the ground state. In DMF, however, the E_{red} values of C_{60} and PBTDP show a shift to the less negative direction by ca. 0.1 V compared to the corresponding values in PhCN; this shift may be related to the observed characteristic photoinduced behavior of fullerene and PBTDP derivatives in highly polar DMF. The electrochemical HOMO−LUMO gap was evaluated to be 1.4 eV in DMF, which is compatible to the value evaluated from MO calculations.

The energy levels (ΔG^0_{RIP}) of the radical ion-pairs such as $C_{60}^{\bullet-}$−PBTDP−$TPA^{\bullet+}$ and $PBTDP^{\bullet-}$−$TPA^{\bullet+}$ were evaluated as a difference between the E_{ox} and E_{red} values, considering the Coulomb energy (ΔG_S) calculated by the Weller equations.[29] The ΔG^0_{RIP} values are listed in Table 2, from which the free-energy changes for charge separation (ΔG^0_{CS}) can be calculated by considering the lowest excited states (ΔE_{0-0}) of the C_{60} (1.75 eV) and PBTDP (2.05−2.50 eV) as shown in eqs 1 and 2.[30]

$$\Delta G^0_{RIP} = -\Delta G^0_{CR} = -E_{ox} + E_{red} - \Delta G_S \qquad (1)$$

$$-\Delta G^0_{CS} = \Delta E_{0-0} - \Delta G^0_{RIP} \qquad (2)$$

Steady-State Absorption Studies. The steady-state absorption spectra of C_{60}−PBTDP−TPA, $NMPC_{60}$, and PBTDP−TPA in toluene are shown in Figure 3. The absorption bands of the BTD and TPA moieties appeared around 320 and 308 nm, respectively. In the case of PBTDP−TPA, the new absorption peak appeared at 413 nm, indicating the ICT transition because the PBTDP and TPA moieties act as an electron-acceptor and an electron-donor, respectively.[31] Therefore, the absorption band of C_{60}−PBTDP−TPA at 408 nm is mainly attributed to the ICT transition within the PBTDP−TPA moiety. The absorption peaks at 705 nm and below 350 nm of C_{60}−PBTDP−TPA are ascribed to the C_{60} moiety.[31] No additional absorption band or no appreciable shift was observed for C_{60}−PBTDP−TPA compared with the sum of the absorptions of $NMPC_{60}$ and

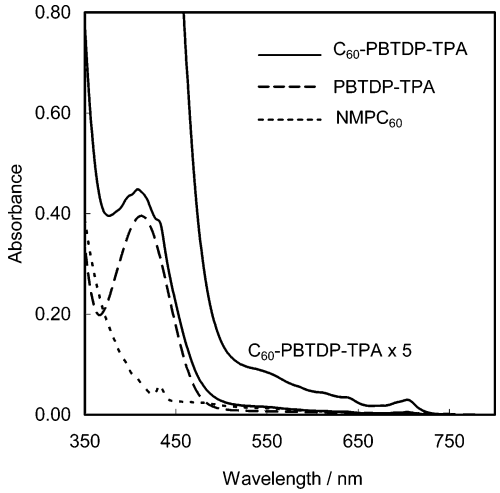

Figure 3. Steady-state absorption spectra of C_{60}−PBTDP−TPA (0.02 mM), $NMPC_{60}$ (0.02 mM), and PBTDP−TPA (0.02 mM) in toluene.

TABLE 2: Free Energies of Radical Ion-Pairs of C_{60}−PBTDP−TPA[a]

solvents	ΔG_{RIP}/eV for $C_{60}^{\bullet-}$−PBTDP−$TPA^{\bullet+}$	ΔG_{RIP}/eV for C_{60}−$PBTDP^{\bullet-}$−$TPA^{\bullet+}$
PhCN	1.49	2.36
DMF	1.43	2.29

[a] ΔG_{RIP} was calculated from the Weller eq 1, in which $\Delta G_S = e^2/(4\pi\epsilon_0\epsilon_R R_{CC})$ in PhCN and DMF.[29]

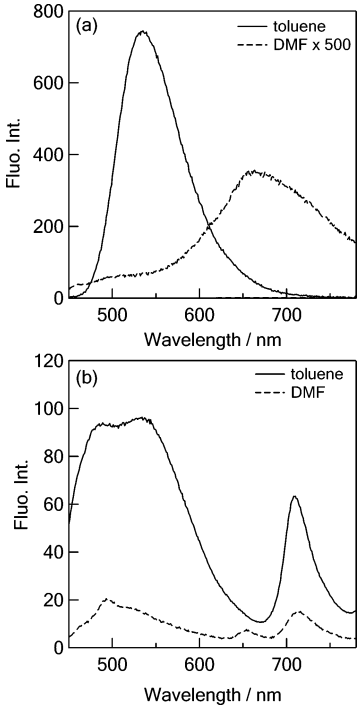

Figure 4. Steady-state fluorescence spectra of (a) PBTDP−TPA (0.01 mM) and (b) C_{60}−PBTDP−TPA (0.01 mM) in toluene and DMF; λ_{ex} = 400 nm.

PBTDP−TPA. This finding suggests that there is no strong interaction in the ground state between the C_{60} and PBTDP−TPA moieties. Similar results were obtained in PhCN and DMF (Supporting Information). By the selection of the laser light wavelength in the fluorescence and transient absorption measurements, the excitation of the C_{60} moiety in C_{60}−PBTDP−TPA and the ICT band of PBTDP−TPA moiety can be controlled on the basis of these absorption bands.

Steady-State Fluorescence Studies. Figure 4a shows steady-state fluorescence spectra of PBTDP−TPA in toluene and DMF observed by the excitation with the 400 nm light, which mainly excites the ICT absorption band of PBTDP−TPA. In toluene, the fluorescence peak appeared at 535 nm with a broad bandwidth spreading in the 500−600 nm region. The steady-state fluorescence at 535 nm in toluene was assigned to the excited ICT, which keeps the molecular structure in the ground state of PBTDP−TPA; from the optimized planar structure in Figure 2, we ascribed this fluorescence from the planar ICT (PICT) state. In PhCN and DMF, the fluorescence peaks shifted to 650 nm leaving a weak fluorescence band around 500 nm, with decreasing total fluorescence intensities, indicating that the fluorescence bands around 650 nm of PBTDP−TPA may be attributed to the TICT state, which was stabilized in polar solvents.[25] The weak 500 nm fluorescent state may be assigned to the PICT state.

Figure 4b shows the fluorescence spectra of C_{60}−PBTDP−TPA; the fluorescence intensities decreased very much by a factor of ca. 1/500 compared with that of PBTDP−TPA even in toluene, suggesting the occurrence of energy transfer (EN) from the ^{1}(PBTDP−TPA)* moiety to the C_{60} moiety of C_{60}−PBTDP−TPA, which can be confirmed by the appearance of the fluorescence peak of the $^1C_{60}$* moiety at 720 nm.[32] In toluene, the PBTDP−TPA moiety in C_{60}−PBTDP−TPA showed broadening of the 535 nm fluorescence band probably by the effect of the C_{60} moiety.

In polar solvent, further decrease in the fluorescence intensity was observed by the comparison with that in toluene, suggesting

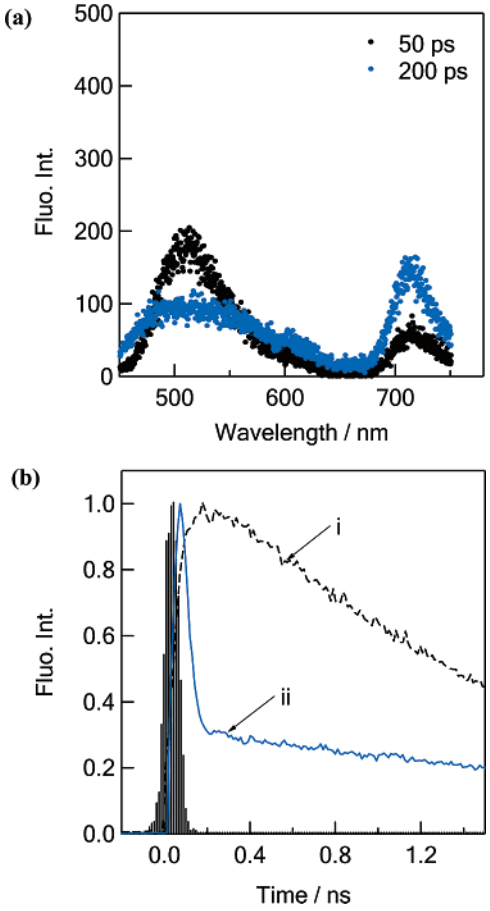

Figure 5. (a) Time-resolved fluorescence spectra of C_{60}−PBTDP−TPA in toluene λ_{ex} = 400 nm. (b) Fluorescence decays of C_{60}−PBTDP−TPA with excitation at 400 nm and detection at (i) 720 nm and (ii) 550 nm in toluene.

that the CS process occurs from C_{60}−^{1}(PBTDP−TPA)*, probably generating $C_{60}^{\bullet-}$−PBTDP−TPA$^{\bullet+}$. Because the fluorescence intensity at 725 nm is decreased in DMF compared with that in toluene, the CS process also takes place via $^1C_{60}$* in C_{60}−PBTDP−TPA. The broad 500 nm fluorescence band of PBTDP−TPA may shift to 530 nm by the effect of the C_{60} moiety.

To estimate the dipole moments of the excited CT and TICT states of C_{60}−PBTDP−TPA, we plotted a Lippert−Mataga equation using the maxima of the PICT and TICT fluorescence in solvents with different polarity (Supporting Information).[33] The dipole moments of the PICT and TICT states were estimated to be 9.0 and 17.5 D, respectively, using the ground-state dipole moment of C_{60}−PBTDP−TPA (5.5 D) calculated by the density function B3LYP/3-21G(*) method. With an increase in the twist angles of the TPA group, the high dipole moment of the excited TICT state of PBTDP−TPA results in a strong stabilization by solvation with polar solvent.

Further quantitative analyses on the fluorescence properties were carried out on the basis of time-resolved fluorescence measurements and fluorescence lifetime measurements.

Time-Resolved Fluorescence Spectra and Fluorescence Lifetime Measurements. The time-resolved fluorescence spectra were in good agreement with the observed steady-state fluorescence spectra of PBTDP−TPA and C_{60}−PBTDP−TPA in toluene with excitation at 400 nm. The time-resolved emission spectra of C_{60}−PBTDP−TPA in toluene as shown in Figure 5a exhibited the fluorescence of ^{1}(PBTDP−TPA)* around 535 nm in the initial time region (50 ps); afterward (100 ps),

TABLE 3: Fluorescence Lifetimes (τ_f), Rate Constant (k_{EN}), Quantum Yield (Φ_{EN}) for Energy Transfer from $C_{60}-{}^1$(PBTDP−TPA)* to C_{60}−(PBTDP−TPA), Rate Constant ($k_{CS}{}^I$), Quantum Yield ($\Phi_{CS}{}^I$), and Free-Energy Changes of Charge Separation ($\Delta G^S{}_{CS}{}^I$) of $C_{60}-{}^1$(PBTDP−TPA)* in Toluene, PhCN, and DMF at Room Temperature

excited states[c]	solvent	τ_f/ps	k_{EN}/s^{-1}	(Φ_{EN})	$k^S{}_{CS}{}^I/s^{-1}$	$\Phi^S{}_{CS}{}^I$	$\Delta G^S{}_{CS}{}^I$/eV
$C_{60}-{}^-$(PBTDP−TPA)*[a]	toluene	83	1.2×10^{10}[b]	0.98[b]	0		−0.22[g]
$C_{60}-{}^1$(PBTDP−TPA)*[c]	PhCN	47	(1.2×10^{10})[d]	0.57[e]	9.3×10^{9}[e]	0.43[f]	0.56[g]
$C_{60}-{}^1$(PBTDP−TPA)*[c]	DMF	42	(1.2×10^{10})[d]	0.50[e]	1.2×10^{10}[e]	0.50[f]	0.62[g]

[a] Fluorescence decay of ^{1}(PBTDP−TPA)* at 535 nm in toluene was fitted with biexponential function giving 83 ps (70%) and 4960 ps (30%). [b] Calculated by eqs 3 and 4, in which $(\tau_f)_{sample}$ and $(\tau_f)_{ref}$ were employed to be 83 and 4600 ps for PBTDP−TPA, respectively. [c] Fluorescence decay at 640 nm. [d] The k_{EN} values in PhCN and DMF are assumed to be equal. [e] $\Phi_{EN} = k_{EN}/[(\tau_{F,triad})^{-1}]_{polar-solvent}$. [g] $\Delta G^S{}_{CS}{}^I$ (via $C_{60}-{}^1$(PBTDP−TPA)*$_{TICT}$) was calculated from the Weller eqs 1 and 2. In toluene, $\Delta G_S = e^2/(4\pi\epsilon_0))[(1/(2R_+) + 1/(2R_-) - 1/R_{cc})/\epsilon_R - (1/(2R_+) + 1/(2R_-))/\epsilon_R]$, where R_+, R_-, and R_{cc} are the radii of cation and anion and center-to-center distance between donor and acceptor, respectively. ϵ_R is the dielectric constant of solvents used for measuring the redox potentials.[29]

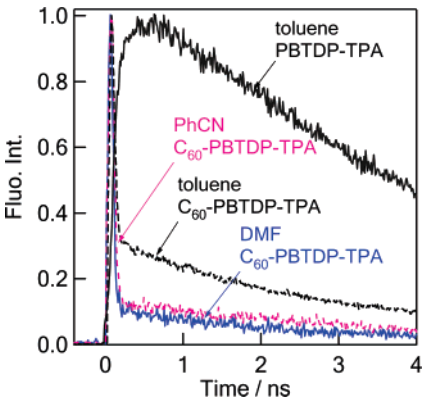

Figure 6. Fluorescence decays of C_{60}−PBTDP−TPA at 550 nm in toluene, at 640 nm in PhCN, and in DMF. Fluorescence decay of PBTDP−TPA at 550 nm in toluene. Excitation at 400 nm.

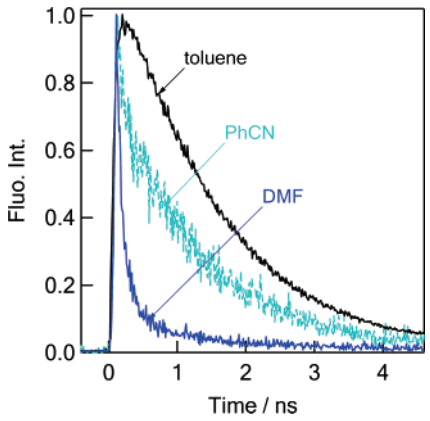

Figure 7. Fluorescence decays of C_{60}−PBTDP−TPA with excitation at 400 nm and detection at 720−750 nm in toluene, PhCN, and DMF.

fluorescence of $^1C_{60}$* appeared at 720 nm, supporting the energy transfer from ^{1}(PBTDP−TPA)* to C_{60}. Furthermore, the relatively sharp fluorescence peak at 500 nm becomes broad at later time region (200 ps), suggesting some changes in the excited state in $C_{60}-{}^1$(PBTDP−TPA)*.

Energy transfer from ^{1}(PBTDP−TPA)* to C_{60} in toluene was further supported by the time profiles shown in Figure 5b, in which the rise of $^1C_{60}$* at 720 nm within 200 ps was observed with concomitant decay of the fluorescence at 550 nm within 200 ps. From the fluorescence time profiles, the lifetimes ($(\tau_f)_{sample}$) were evaluated by the exponential curve-fitting. The rate (k_{EN}) and quantum (Φ_{EN}) for energy transfer can be calculated by eqs 3 and 4, in which the fluorescence lifetime of ^{1}(PBTDP−TPA)* in toluene was used as a reference $(\tau_f)_{ref}$.

$$k_{EN} = (1/\tau_f)_{sample} - (1/\tau_f)_{ref} \quad (3)$$

$$\Phi_{EN} = [(1/\tau_f)_{sample} - (1/\tau_f)_{ref}]/(1/\tau)_{sample} \quad (4)$$

Time resolved-fluorescence spectra of C_{60}−PBTDP−TPA in PhCN and DMF are quite similar to that in toluene (Figure 5) except that the decaying fluorescence peaks are dual fluorescence at 500 and 650 nm (Supporting Information). The observation of the fluorescence of the $^1C_{60}$* moiety at 100 ps suggests that EN takes place even in polar solvent.

In Figure 6, the time profiles in PhCN and DMF show predominant rapid decay; from the major quick decay, the τ_f values of $C_{60}-{}^1$(PBTDP−TPA)*$_{TICT}$ were evaluated to be 42−47 ps, whereas minor slow decay components (less than 10%) gave the τ_f value of 2500−5000 ps. The fluorescence of PBTDP−TPA in toluene shown as reference sample in Figure 6 exhibited the rise in the initial time (0−500 ps) followed by the slow decay with the τ_f value of 4600 ps. When the solvent polarity effect on the k_{EN} values is small, we can assume the same k_{EN} values for all solvents. However, the quantum yields of energy transfer in polar solvents, which can be calculated by eq 5, decrease with the solvent polarity as shown in Table 3.

$$\Phi_{EN} = k_{EN}/[(\tau_{F,triad})^{-1}]_{polar-solvent} \quad (5)$$

Thus, the CS process from $C_{60}-{}^1$(PBTDP−TPA)* to generate $C_{60}{}^{\bullet-}$−PBTDP−TPA$^{\bullet+}$, which refers to the $k_{CS}{}^I$ and $\Phi_{CS}{}^I$ values, can be evaluated by eqs 6 and 7.

$$k^S{}_{CS}{}^I = (1/\tau_f)_{polar-solvent} - k_{EN} \quad (6)$$

$$\Phi^S{}_{CS}{}^I = k^S{}_{CS}{}^I/(1/\tau_f)_{polar-solvent} \quad (7)$$

These values are also listed in Table 3. From the negative $\Delta G^S{}_{CS}{}^I$ values in polar solvents, the CS processes via the ^{1}(PBTDP−TPA)*$_{TICT}$ moieties in C_{60}−PBTDP−TPA are thermodynamically favorable.

In toluene, the fluorescence time profile of $^1C_{60}$*−PBTDP−TPA at 710 nm observed in long time-scale measurements shows single-exponential decay after quick rise as shown in Figure 7. From the single-exponential decay, the fluorescence lifetime (τ_f) was evaluated to be 1480 ps, which is nearly equal to that of $NMPC_{60}$ (1300 ps),[32] suggesting that CS does not occur via $^1C_{60}$* in toluene. In PhCN, the τ_f value of $^1C_{60}$*−PBTDP−TPA was evaluated to be 880 ps by a single-exponential decay. In DMF, the time profile shows biexponential decay; the major contribution (95%) was the fast decay component (150 ps) and the slow decay component (ca. 1180 ps) with minor contribution (5%) (Figure 7). From these τ_f values, the rate constant ($k^S{}_{CS}{}^{II}$) and the quantum yield ($\Phi^S{}_{CS}{}^{II}$) for the CS processes via $^1C_{60}$*−PBTDP−TPA were calculated by eqs 3 and 4, in which the $(\tau_f)_{sample}$ and $(\tau_f)_{ref}$ are replaced by the fluorescence lifetimes of $^1C_{60}$* in sample and reference, respectively,[9−13] as listed in Table 4. The $k^S{}_{CS}{}^{II}$ and $\Phi^S{}_{CS}{}^{II}$ values

TABLE 4: Fluorescence Lifetimes (τ_f), Rate Constant (k_{CS}^{II}),[a] Quantum Yield (Φ_{CS}^{II}),[a] and Free-Energy Changes of Charge Separation ($\Delta G^{S}_{CS}{}^{II}$)[b] of $^1C_{60}$*−PBTDP−TPA in Toluene, PhCN, and DMF at Room Temperature

excited state	solvents	τ_f/ps	$k^{S}_{CS}{}^{II}/s^{-1}$	$\Phi^{S}_{CS}{}^{II}$	$-\Delta G^{S}_{CS}{}^{II}$/eV
$^1C_{60}$*−PBTDP−TPA[c]	toluene	1480			−0.52
$^1C_{60}$*−PBTDP−TPA[c]	PhCN	880	4.6×10^8	0.41	0.26
$^1C_{60}$*−PBTDP−TPA[c]	DMF	150	6.0×10^9	0.89	0.32

[a] Calculated by eqs 3 and 4; $(\tau_f)_{ref}$ were calculated to be 1480 ps in toluene. [b] $\Delta G^{S}_{CS}{}^{II}$ via $^1C_{60}$*−PBTDP−TPA.[29] [c] Fluorescence decays of C_{60} (720−750 nm).

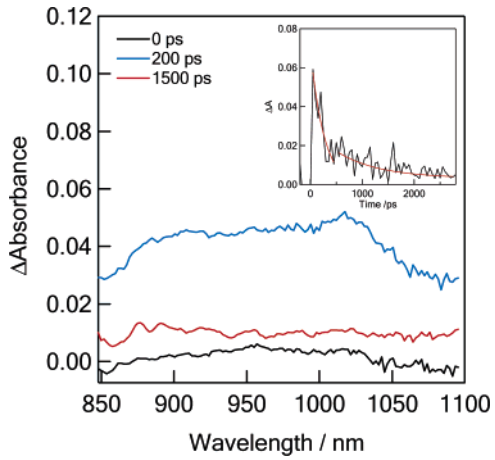

Figure 8. Picosecond transient absorption spectra of C_{60}−PBTDP−TPA (0.1mM) after 390 nm laser irradiation. Inset: Absorption−time profiles at 1000 nm in (a) PhCN.

in DMF are larger than the corresponding values in PhCN, suggesting that the CS process via $^1C_{60}$* belongs to the normal region of the Marcus parabola.[16]

Time-Resolved Transient Absorption Spectra. Picosecond transient absorption spectra observed by the 390 nm laser light excitation of C_{60}−PBTDP−TPA in PhCN are shown in Figure 8. In the spectrum observed at 200 ps, the broad absorption bands appeared with the peaks at 1020 and 900 nm, in which the 1020 nm is the diagnostic evidence for the radical anion of the C_{60} moiety ($C_{60}^{\bullet-}$).[31] The 900 nm band can be assigned to the overlapped band of transition the radical cation of the PBTDP−TPA moiety and the second absorption of the $C_{60}^{\bullet-}$ moiety. These absorption bands reach a maximum about 50−100 ps (in inset of Figure 8), suggesting that the absorption of S_1-S_n transition centered at 900 nm is also overlapping. After reaching a maximum, these absorption bands of the CS state began to decrease with two components, which showed initial rapid decay within 500 ps and subsequent slow decay within ca. 3 ns. Quite similar transient absorption spectra and time profiles were observed in DMF. These observations suggest that the charge-separated states generated via the singlet excited states decay almost completely with 3−4 ns. These decays can be attributed to the charge-recombination (CR) to the ground state; the rate constants (k_{CR}^{S}) are listed in Table 5. Suffix S implies that the CS state formed via the excited singlet states has the singlet spin-character. As the reason of the two-step decay, we can consider that there are two positions of the radical cation; that is $C_{60}^{\bullet-}$−PBTDP$^{\bullet+}$−TPA for the faster decay and $C_{60}^{\bullet-}$−PBTDP−TPA$^{\bullet+}$ for the slower decay, although they could not be discriminated by the broad picosecond transient absorption spectra. In Table 5 are listed the k_{CR}^{S} values evaluated from slower decays.

In the nanosecond transient spectrum of C_{60}−PBTDP−TPA in DMF (Figure 9), the transient absorption bands appeared

TABLE 5: Charge-Recombination Rate Constants (k_{CR}), Lifetimes of Charge Recombination (τ_{RIP}), and Free Energy of Charge Recombination (ΔG^0_{CR}) of C_{60}−PBTDP−TPA in PhCN and DMF at Room Temperature

compd	solvent	$k_{CR}^{S}{}^{a}/s^{-1}$	$k_{CR}^{T}{}^{b}/s^{-1}$	$\tau_{RIP}/\mu s$	ΔG^0_{CR}/eV
$C_{60}^{\bullet-}$−PBTDPTPA$^{\bullet+}$	PhCN	8.8×10^9	1.3×10^4	76.9	−1.49
$C_{60}^{\bullet-}$−PBTDP−TPA$^{\bullet+}$	DMF	1.5×10^9	7.5×10^5	1.4	−1.43

[a] From the slower decay part of the picosecond transient spectra (see Figure 8). [b] From the slower decay part of the nanosecond transient spectra (see Figures 9 and 10).

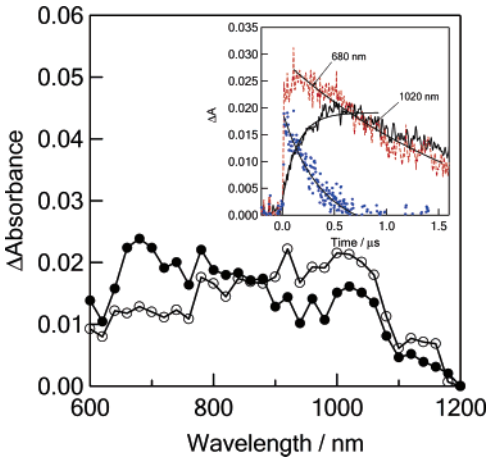

Figure 9. Nanosecond transient absorption spectra of C_{60}−PBTDP−TPA (0.1 mM) at 0.1 μs (●) and 1.0 μs (○) after 450 nm laser irradiation. Inset: Absorption−time profiles at 680 nm (red) 1020 nm (black) and at 680 nm (blue) subtracted time profile from 1020 nm in DMF.

around 850−1000 nm, which are quite similar to those observed in the picosecond transient absorption spectrum (Figure 8). Thus, generation of $C_{60}^{\bullet-}$−PBTDP−TPA$^{\bullet+}$ by the excitation of the PBTDP-TPA moiety (450 nm laser light) in C_{60}−PBTDP−TPA can be confirmed in DMF. By the excitation of the C_{60} moiety in C_{60}−PBTDP−TPA with 532 nm laser light, similar transient absorption spectra of $C_{60}^{\bullet-}$−PBTDP−TPA$^{\bullet+}$ were also observed in DMF (Supporting Information). The absorption band at 680 nm showing only decay after the 6 ns laser pulse can be attributed to the absorption band of the radical cation of the TPA$^{\bullet+}$ moiety, to which a small amount of the absorption of the $^3C_{60}$* moiety may be overlapping.

The time profile (Figure 9) at 1020 nm in DMF shows the slow rise after the 6 ns laser excitation reaching to the maximum at ca. 500 ns. The slow rise of the $C_{60}^{\bullet-}$ moiety in $C_{60}^{\bullet-}$−PBTDP−TPA$^{\bullet+}$ may be explained by the second CS process that takes place via the triplet states. Although the $\Phi^{S}_{CS}{}^{II}$ value is larger than 0.90, the $\Phi^{S}_{CS}{}^{I}$ value is less than 0.5 (Table 4); therefore, the slow charge-separations via the ^{3}(PBTDP−TPA)* and $^3C_{60}$* moieties are possible. From the curve-fitting with a single-exponential rise part at 1000 nm, the CS rate constant (k_{CS}^{T}) via the triplet states in C_{60}−PBTDP−TPA was calculated to be 6.5×10^6 s^{-1}. The absorption band at 680 nm showing only decay after the 6 ns laser pulse can be attributed the $^3C_{60}$* moiety, with which the absorption band of the radical cation of the TPA$^{\bullet+}$ moiety may be overlapped. From the curve-resolving of the time profile with the decay of the $^3C_{60}$* moiety and the rise of the TPA$^{\bullet+}$ moiety as shown inset in Figure 9, the decay was evaluated to be 2.7×10^6 s^{-1}, which is in good agreement with the rise of the $C_{60}^{\bullet-}$ moiety evaluated from the 1000 nm band.

After reaching a maximum, the absorption band at 1000 nm began to decay with obeying first-order kinetics with rate

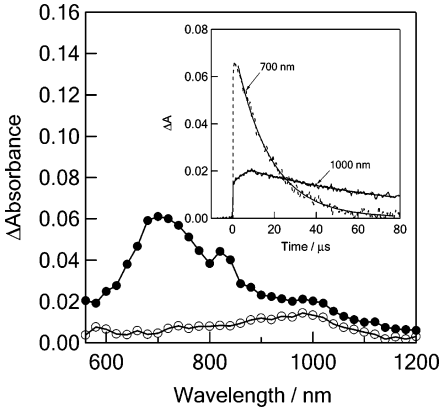

Figure 10. Nanosecond transient absorption spectra of C_{60}−PBTDP−TPA (0.1 mM) at 5 μs (●) and 50 μs (○) after 450 nm laser irradiation. Inset: Absorption−time profiles at 700 and 1000 nm in PhCN.

constants of 7.5×10^5 s^{-1} at room temperature. This decay process is attributed to the CR process from $C_{60}^{\bullet-}$−PBTDP−$TPA^{\bullet+}$ with the triplet spin character in DMF; thus, the observed rate constant is attributed to k_{CR}^T. From the inverse of the k_{CR}^T values, the lifetime (τ_{RIP}) of the radical ion-pair $C_{60}^{\bullet-}$−PBTD−$TPA^{\bullet+}$ was evaluated to be 1430 ns in DMF at room temperature. The k_{CR}^T values are extremely smaller than the k_{CR}^S values because the triplet spin character of the CS state needs a considerable spin-inversion times to go the ground state.[9b,34]

Figure 10 shows the nanosecond transient absorption spectra in PhCN. The absorption bands of the CS state was not appreciable seen in the initial time, since the absorption bands of $C_{60}^{\bullet-}$−PBTDP−$TPA^{\bullet+}$ are hidden by the intense absorption of $^3C_{60}$*−PBTDP−TPA. As shown in time profiles measured in longer time scale, with concomitant the decay of the $^3C_{60}$* moiety at 700 nm, the rise of the $C_{60}^{\bullet-}$ moiety at 1000 nm was observed in the time region of 0−10 μs, which corresponds to the CS process via the $^3C_{60}^*$ moiety of C_{60}−PBTDP−TPA in PhCN ($k_{CS}^T = 1.5 \times 10^5$ s^{-1}). After reaching a maximum at 10 μs, the $C_{60}^{\bullet-}$ moiety decay slower than the decay of the $^3C_{60}$* moiety.[35] Therefore, the transient absorption spectrum depicted at 50 μs is quite similar to that of $C_{60}^{\bullet-}$−PBTDP−$TPA^{\bullet+}$. Thus, the decay of $C_{60}^{\bullet-}$−PBTDP−$TPA^{\bullet+}$ can be attributed to k_{CR}^T values, from which the τ_{RIP} was evaluated to be 80 μs in PhCN. This τ_{RIP} in PhCN is longer than that in DMF, which is reasonable trend along with the inverted region of the Marcus parabola.[36]

Energy Diagrams. From the ΔG^0_{CR} and ΔG^0_{CS} values in Table 2, the energy diagram for C_{60}−PBTDP−TPA can be illustrated as shown in Figure 11, in which the E_{0-0} values of $^1C_{60}$* and $^3C_{60}$* are adopted the reported values of 1.75 and 1.50 eV, respectively. The energy levels of $C_{60}^{\bullet-}$−PBTDP−$TPA^{\bullet+}$ depend on the solvent polarity. Therefore, since the CS state of C_{60}−PBTDP−TPA in toluene is higher than the $^1C_{60}$* state, no CS process via the $^1C_{60}$* state takes place, resulting in the observation of the absorption of $^3C_{60}$* with long lifetime than 20 μs.[31] In polar solvents, the CS process via $^1C_{60}$* is possible.

Short lifetimes of C_{60}−^{1}(PBTDP−TPA)* in nonpolar solvents suggest that the EN process predominantly takes place. In polar solvents, the direct CS process takes place generating $C_{60}^{\bullet-}$−PBTDP−$TPA^{\bullet+}$ in addition to the EN process. Thus, $C_{60}^{\bullet-}$−PBTDP−$TPA^{\bullet+}$ can be generated via the $^1C_{60}$* state formed by the direct excitation and indirectly via EN process from C_{60}−^{1}(PBTDP−TPA)*$_{TICT}$. However, the transient absorption spectra from the picosecond to microsecond time region indicate the lifetime of $C_{60}^{\bullet-}$−PBTDP−$TPA^{\bullet+}$ produced via these excited singlet states are short.

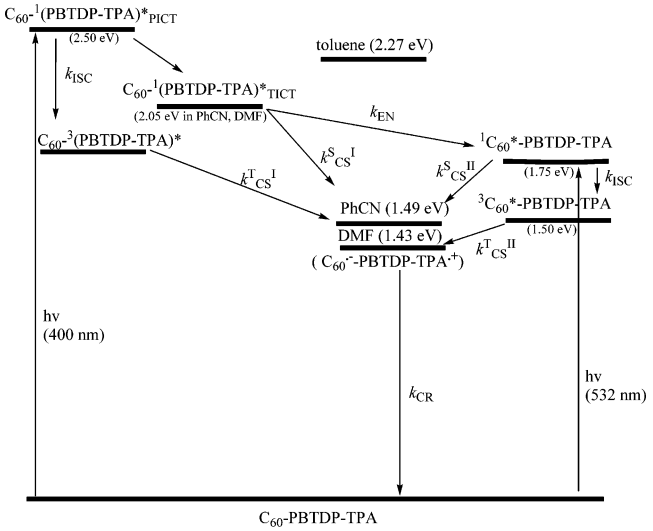

Figure 11. Energy diagram of C_{60}−PBTDP−TPA.

Since the $^3C_{60}$* state is slightly higher than the states of $C_{60}^{\bullet-}$−PBTDP−$TPA^{\bullet+}$ in PhCN and DMF, the CS process via the $^3C_{60}$* state is possible, too. Extremely slow k_{CS}^T value in PhCN is reasonable because of the small energy difference between the $^3C_{60}$* state and the CS state. The CS process via C_{60}−^{3}(PBTDP−TPA)* is possible, since its energy is higher than that of the $^3C_{60}$* state; however, the contribution to the CS process is not so clearly shown, because the transient absorption bands of ^{3}(PBTDP−TPA)* appears in the 800−900 nm region.

Since the CR process with large ΔG_{CR} in PhCN was slower than that with a smaller ΔG_{CR} value in DMF, the CR process may belong to the inverted region of the Marcus parabola because of the small reorganization energy is characteristic of the fullerene derivatives.[16c,d]

Comparison with Other Dyads and Triads. In the CR process, long τ_{RIP} values were reported for C_{60}−amine donor dyads in DMF at room temperature. For example, the τ_{RIP} value for a dyad composed of the C_{60}−(fluorene−diphenylamine) was evaluated to be 150 ns in DMF at room temperature.[15] In the case of C_{60}−bridge−dimethylaniline systems, the τ_{RIP} values in the range of 8−250 ns were reported, depending on the kinds and lengths of the bridge molecules.[7a,b] Compared with these C_{60} and amine dyads, $C_{60}^{\bullet-}$−PBTDP−$TPA^{\bullet+}$ in DMF showed the longest τ_{RIP} value among the C_{60} connected with aromatic amine systems using various bridges in solutions. Comparison of the τ_{RIP} values in PhCN is quite difficult, because the overlapping of the absorptions of $C_{60}^{\bullet-}$ and $^3C_{60}$* prohibited the accurate evaluation of the τ_{RIP} values in PhCN. In the case of $C_{60}^{\bullet-}$−PBTDP−$TPA^{\bullet+}$, the evaluation of the τ_{RIP} value was possible, because of the τ_{RIP} value was longer than the lifetimes of the $^3C_{60}$* moiety in C_{60}−PBTDP−TPA.

In other systems such as porphyrins connected with C_{60} and chlorins connected with C_{60} systems, longer lifetimes were recently reported at low temperature in the rigid media by following the EPR signals.[37] Therefore, there remains to design other aromatic-amine connected C_{60} systems based on the data described in these studies.

This τ_{RIP} value for C_{60}−PBTDP−TPA is significantly longer than those reported τ_{RIP} values for the C_{60}−(BTD−TPA), in which the radical cation (hole) delocalizes in the (BTD−TPA) moiety.[27] However, the HOMO and LUMO calculations of the present work clearly show that there is no radical cation (hole) delocalization in C_{60}−PBTDP−TPA because of introduction of phenyl group between BTD and TPA.

The highly dipolar nature of the TICT state leads to a high sensitivity toward solvent polarity. The advantageous property of moderately twisted C_{60}−PBTDP−TPA to combine high fluorescence quantum yields with large stokes-shifts is proposed for the effective electron donor in the charge-separation process of C_{60}−PBTDP−TPA in polar solvents. The twisting character of PBTDP−TPA may also affect on the electron transfer from the C_{60} to the TPA to retard the charge-recombination process.

Conclusions

For [60]fullerene covalently linked to PBTDP−TPA, photoinduced CS and EN processes take place via both $^1C_{60}$* and ^{1}(PBTDP−TPA)* moieties producing the ultimate CS state $C_{60}^{\bullet-}$−PBTDP−$TPA^{\bullet+}$ in polar solvent. The PBTDP moiety with TPA moiety acts as a good electron-donor, light-harvesting antenna, and an efficient energy-mediating reagent to the C_{60} moiety. In the electron-transfer step, the TPA moiety acts as an electron donor. The PBTDP−TPA moiety increases the efficiency of the CS process and the lifetimes of the CS state in polar solvents. The importance of the spin state of the precursor to attain the long-lived ion-pair formation was revealed. The role of the PBTDP−TPA in the CS process and CR process may be complex and difficult to disclose explicitly, although various clues could be obtained from the complex fluorescence spectral shift and time profiles.

Experimental Section

General Methods. All melting points are uncorrected. IR spectra were recorded on a JASCO FT/IR-470 plus Fourier transform infrared spectrometer and measured as KBr pellets. ^{1}H NMR spectra were determined in $CDCl_3$ with a JEOL EX-270 spectrometer. Residual solvent protons were used as internal standard, and chemical shifts (δ) are given relative to tetramethylsilane (TMS). The coupling constants (J) are reported in Hz. Elemental analysis was performed at the Elemental Analytical Center, Kyushu University. Electron impact mass spectrometry (EI-MS) spectra were recorded with a JEOL JMS-70 mass spectrometer at 70 eV using a direct inlet system. Fast atom bombardment mass spectrometry (FAB-MS) was recorded with a JEOL JMS-70 mass spectrometer with *m*-nitrobenzyl alcohol (NBA) as a matrix. Gel permeation chromatography (GPC) was performed with a Japan Analytical Industry Co., Ltd LC-908 using JAIGEL-1H column (20 × 600 mm) and JAIGEL-2H column (20 × 600 mm) eluting with chloroform (3.0 mL/min). Analytical TLC was carried out on silica gel coated on aluminum foil (Merck 60 F_{254}). Column chromatography was carried out on silica gel (KANTO 60N). Compounds $NMPC_{60}$,[28] PBTDP,[21] and **1**[38] were prepared according to the methods reported previously.

2,2-Dimethyl-1,3-propanediol 4′-(Diphenylamino)biphenyl-4-boronate. A mixture of 4,4′-diiodobiphenyl (6.0 g, 14.9 mmol), diphenylamine (2.28 g, 13.5 mmol), copper powder (109 g, 1.72 mmol), and potassium carbonate (1.86 g, 13.5 mmol) in *o*-xylene (15 mL) was heated at 170 °C for 12 h under an argon atmosphere. The reaction mixture was diluted with toluene (110 mL) at room temperature, and then it was heated at refluxing temperature for 4 h. The reaction mixture was filtered over Celite and washed with toluene. The filtrate was evaporated in vacuo to dryness. The residue was suspended in chloroform, and the insoluble 4,4′-diiodobiphenyl was removed by filtration. The filtrate was evaporated in vacuo to dryness. The residue was purified by silica gel column chromatography eluting with *n*-hexane/chloroform (9:1, v/v) to give 4-diphenylamino-4′-iodobiphenyl in 27% yield (1.60 g, 3.58 mmol) as a white solid: mp 143−144 °C; IR (KBr, cm^{-1}) 1587, 1516, 1476, 1328, 1276, 996, 812, 749, 695, 514; ^{1}H NMR ($CDCl_3$) δ 7.04 (t, J = 7.2 Hz, 2 H, ArH), 7.10−7.14 (m, 6 H, ArH), 7.24−7.32 (m, 6 H, ArH), 7.42 (d, J = 8.3 Hz, 2 H, ArH), 7.72 (d, J = 7.9 Hz, 2 H, ArH).

To a solution of 4-diphenylamino-4′-iodobiphenyl (2.10 g, 4.7 mmol) in dry THF (35 mL) added 1.59 M *n*-butyllithium hexane solution (3.53 mL, 5.62 mmol) for 40 min at −78 °C under an argon atmosphere. After the mixture was allowed to stand for 1 h, tri(isopropyl)borate (1.1 mL, 7.39 mmol) in dry THF (14 mL) was added for 20 min at −78 °C. The reaction mixture was stirred for an additional 1 h and allowed to warm to room temperature for 1.5 h. After the reaction mixture was quenched by addition with aqueous 1.2 N HCl solution (to pH 5−7), it was extracted with ether. The combined organic layers were washed with aqueous sodium thiosulfate solution and water, dried over anhydrous magnesium sulfate, and evaporated in vacuo to give crude 4′-(diphenylamino)biphenyl-4-boronic acid.

The residue and 2,2-dimethyl-1,3-propanediol (535 mg, 5.1 mmol) were dissolved in dichloromethane (19 mL) and stirred at room temperature for 4 h under an argon atmosphere. The reaction mixture was dried over anhydrous magnesium sulfate and evaporated in vacuo to dryness. The residue was purified by silica gel column chromatography eluting with *n*-hexane/chloroform (1:4, v/v) to give 2,2-dimethyl-1,3-propanediol 4′-(diphenylamino)biphenyl-4-boronate in 44% yield (980 mg, 2.26 mmol) as a white solid: mp 202−203 °C; IR (KBr, cm^{-1}) 3035, 2956, 1591, 1523, 1492, 1423, 1378, 1319 (ν_{BO}), 1283, 1246, 1133, 823, 754, 696, 649, 512; ^{1}H NMR ($CDCl_3$) δ 1.03 (s, 6 H, CH_3), 3.78 (s, 4 H, CH_2), 7.02 (t, J = 7.2 Hz, 2 H, ArH), 7.10−7.14 (m, 6 H, ArH), 7.23−7.29 (m, 4 H, ArH), 7.50 (d, J = 6.7 Hz, 2 H, ArH), 7.57 (d, J = 8.1 Hz, 2 H, ArH), 7.84 (d, J = 8.1 Hz, 2 H, ArH); EI-MS (positive, NBA) *m*/*z* 433 (M^+). Anal. Calcd for $C_{29}H_{28}BNO_2$: C, 80.38; H, 6.51; N, 3.23. Found: C, 80.16; H, 6.43; N, 3.22.

4-Bromo-7-(4-formylphenyl)-2,1,3-benzothiadiazole (2). To a mixture of **1** (2.10 g, 7.1 mmol) and tetrakis(triphenylphosphine)palladium (0) (201 mg, 0.17 mmol) in benzene (70 mL) were added 4-formylphenylboronic acid (1.21 g, 8.1 mmol), ethanol (18 mL), and aqueous 2 M sodium carbonate solution (35 mL) at 60 °C under an argon atmosphere. After the mixture was heated at 80 °C for 4 h, the reaction mixture was poured into brine and extracted with dichloromethane. The combined organic layers were washed with brine, dried over anhydrous magnesium sulfate, and evaporated in vacuo to dryness. The residue was purified by silica gel column chromatography eluting with chloroform to give **2** in 28% yield (638 mg, 2.0 mmol) as a pale yellow powder: mp 205−206 °C; IR (KBr, cm^{-1}) 3085, 2815, 2726, 1696 ($\nu_{C=O}$), 1603, 1530, 1480, 1420, 1308, 1216, 1151, 934, 881, 838, 820, 677, 554, 517, 499, 464; ^{1}H NMR($CDCl_3$) δ 7.66 (d, J = 7.6 Hz, 1 H, ArH), 7.97 (d, J = 7.6 Hz, 1 H, ArH), 8.03 (d, J = 6.4 Hz, 2 H, ArH), 8.09 (d, J = 6.4 Hz, 2 H, ArH), 10.10 (s, 1 H, CHO); EI-MS (positive, NBA) *m*/*z* 318, 320 (M^+). Anal. Calcd for $C_{13}H_7BrN_2OS$: C, 48.92; H, 2.21; N, 8.78. Found: C, 49.15; H, 2.27; N, 8.86.

4-[4′-(Diphenylamino)biphenyl-4-yl]-7-(4-formylphenyl)-2,1,3-benzothiadiazole (3). According to a method similar to the preparation of **2**, **3** was obtained in 35% yield (79 mg, 0.14 mmol) from **2** (128 mg, 0.4 mmol), tetrakis(triphenylphosphine)-palladium (0) (14 mg, 0.012 mmol), benzene (4 mL), 2,2-dimethyl-1,3-propanediol (diphenylamino)biphenyl-4-boronate (208 mg, 0.48 mmol), ethanol (1 mL), and aqueous 2 M sodium carbonate solution (2 mL). The reaction was performed at 80

°C for 2.5 h. The crude product was purified by silica gel column chromatography (*n*-hexane/chloroform, 1:2 (v/v)): yellow powder; mp 220−221 °C; IR (KBr, cm^{-1}) 3028, 2360, 1694($\nu_{C=O}$), 1590, 1490, 1315, 1289, 1266, 1212, 1170, 887, 820, 750, 702, 696, 521; ^1H NMR ($CDCl_3$) δ 7.05 (t, J = 7.2 Hz, 2 H, ArH), 7.14−7.18 (m, 6 H, ArH), 7.25−7.32 (m, 4 H, ArH), 7.57 (d, J = 8.4 Hz, 2 H, ArH), 7.77 (d, J = 8.4 Hz, 2 H, ArH,), 7.87 (d, J = 7.4 Hz, 1 H, ArH), 7.90 (d, J = 7.4 Hz, 1 H, ArH), 8.05 (d, J = 8.4, 2 H, ArH), 8.06 (d, J = 8.4, 2 H, ArH), 8.18(d, J = 8.4 Hz, 2 H, ArH), 10.10 (s, 1 H, CHO); FAB-MS (positive, NBA) *m*/*z* 559 (M^+). Anal. Calcd for $C_{37}H_{25}N_3OS \cdot 0.2CHCl_3$: C, 76.56; H, 4.35; N, 7.20. Found: C, 76.98; H, 4.43; N, 7.25.

[60]Fullerene−Diphenybenzothiadiazole−Triphenylamine Triad (C_{60}−PBTDP−TPA). A solution of [60]fullerene (72 mg, 0.10 mmol), *N*-methylglycine (11 mg, 0.12 mmol), and **3** (56 mg, 0.10 mmol) in *p*-xylene (20 mL) was heated at the refluxing temperature for 5 h under an argon atmosphere. After the reaction mixture was cooled to room temperature, the solvent was removed in vacuo to dryness. The residue dissolved in 1,2-dichlorobenzene was subjected to silica gel column chromatography eluting with toluene/*n*-hexane (4:1, (v/v)) to give C_{60}−PBTDP−TPA in 23% yield (29 mg, 0.023 mmol) as a brown solid: mp > 450 °C; IR (KBr cm^{-1}) 2922, 1589, 1480, 1330, 1278, 818, 751, 694, 669, 526; ^1H NMR ($CDCl_3/CS_2$, 19:1 (v/v)) δ 2.89 (s, 3 H, CH_3), 4.33 (d, J = 9.3 Hz, 1 H, CH_2), 5.04 (d, J = 9.3 Hz, 1 H, CH_2), 5.05 (s, 1 H, CH), 7.04 (t, J = 7.2 Hz, 2 H, ArH), 7.21−7.30 (m, 12 H, ArH), 7.54 (d, J = 8.7 Hz, 2 H, ArH), 7.72 (d, J = 8.4 Hz, 2 H, ArH), 7.82 (d, J = 7.4 Hz, 1 H, ArH), 7.85 (d, J = 7.4 Hz, 1 H, ArH), 8.03 (d, J = 8.4 Hz, 2 H, ArH), 8.12 (d, J = 8.7 Hz, 2H, ArH); FAB-MS (positive, NBA) *m*/*z* 1307 (M^+). Anal. Calcd for $C_{99}H_{30}N_4S \cdot C_7H_8$: C, 90.97; H, 2.74; N, 4.00. Found: C, 90.60; H, 2.93; N, 4.05.

4-Bromo-7-(4-tolyl)-2,1,3-benzothiadiazole (4). According to a method similar to the preparation of **2**, **4** was obtained as inseparable mixture with **1** and 4,7-bis(4-tolyl)-2,1,3-benzothiadiazole (**4**/**1**/bis-product = 57:26:17, mol/mol/mol) from **1** (500 mg, 1.7 mmol), tetrakis(triphenylphosphine)palladium (0) (59 mg, 0.05 mmol), benzene (19 mL), 4-tolylboronic acid (367 mg, 1.8 mmol), ethanol (4.8 mL), and aqueous 2 M sodium carbonate solution (9.5 mL). The reaction was performed at 80 °C for 3 h. The crude product was separated by silica gel column chromatography (*n*-hexane/chloroform, 2:1 (v/v)). Without further purification, **4** was used in the next reaction: ^1H NMR ($CDCl_3$) δ 2.44 (s, 3 H, CH_3), 7.34 (d, J = 8.1 Hz, 2 H, ArH), 7.56 (d, J = 7.6 Hz, 2 H, ArH), 7.79 (d, J = 8.1 Hz, 2H, ArH), 7.91 (d, J = 7.6 Hz, 2H, ArH).

4-[4′-(Diphenylamino)biphenyl-4-yl]-7-(4-tolyl)-2,1,3-benzothiadiazole (PBTDP−TPA). According to a method similar to the preparation of **2**, PBTDP−TPA was obtained in 31% yield (80 mg, 0.15 mmol) from **4** (purity of 57 mol %, 147 mg, 0.48 mmol), tetrakis(triphenylphosphine)palladium (0) (16 mg, 0.014 mmol), benzene (5 mL), 2,2-dimethyl-1,3-propanediol (diphenylamino)biphenyl-4-boronate (220 mg, 0.53 mmol), ethanol (1.2 mL), and aqueous 2 M sodium carbonate solution (2.4 mL). The reaction was performed at 80 °C for 16 h. The crude product was purified by silica gel column chromatography (*n*-hexane/chloroform, 2:1 (v/v)) and by GPC (chloroform): yellow solid; mp 214−216 °C; IR (KBr, cm^{-1}) 1588, 1494, 1484, 1325, 1269, 894, 814, 751, 696, 620, 535, 518; ^1H NMR ($CDCl_3$) δ 2.45 (s, 3 H, CH_3), 7.05 (t, J = 7.3 Hz, 2 H, ArH), 7.14−7.18 (m, 6 H, ArH), 7.25−7.31(m, 4 H, ArH), 7.36 (d, J = 8.2 Hz, 2 H, ArH), 7.56 (d, J = 8.6 Hz, 2 H, ArH), 7.74 (d, J = 8.1 Hz, 2H, ArH), 7.79, 7.81 (d, J = 6.4 Hz, each 1H, ArH), 7.88 (d, J = 8.1 Hz, 2 H, ArH), 8.04 (d, J = 8.2 Hz, 2 H, ArH); FAB-MS (positive, NBA) *m*/*z* 545 (M^+). Anal. Calcd for $C_{37}H_{27}N_3S \cdot 0.1CHCl_3$: C, 79.91; H, 4.90; N, 7.54. Found: C, 79.72; H, 5.00; N, 7.47.

Spectral Measurements. Time-resolved fluorescence spectra were measured by a single-photon counting method using a second harmonic generation (SHG, 400 nm) of a Ti:sapphire laser [Spectra-physics, Tsunami 3950-L2S, 150 fs full width at half-maximum (fwhm)] and a streak scope (Hamamatsu Photonics, C4334−01) equipped with a polychromator (Action Reasearch, SpectraPro 150) as an excitation source and a detector, respectively.[39]

The femtosecond transient absorption spectra were measured by the pump and probe method using a Ti:sapphire regenerative amplifier seeded by the SHG of an Er-doped fiber laser (Clark-MXR CPA-2001 plus, 1 kHz, fwhm 150 fs). A white continuum pulse used as a monitoring light was generated by focusing the fundamental of the amplifier on a rotating H_2O cell. The samples were excited by the SHG (388 nm) of fundamental. The monitoring light transmitted through the sample in a rotating cell was detected with a dual MOS detector (Hamamatsu Photonics, C6140) equipped with a polychromator for the visible region or an InGaAs linear image sensor (Hamamatsu Photonics, C5890-128) for the near-IR region. A typical time resolution of the system is 200 fs.

Nanosecond transient absorption measurements were carried out using OPA (450 nm) and SHG (532 nm) of Nd:YAG laser (Spectra Physics, Quanta-Ray GCR-130, fwhm 6 ns) as an excitation source. For transient absorption spectra in the near-IR region (600−1600 nm), monitoring light from a pulsed Xe lamp was detected with a Ge-avalanche photodiode (Hamamatsu Photonics, B2834). Photoinduced events in micro- and millisecond time regions were estimated by using a continuous Xe lamp (150 W) and an InGaAs-PIN photodiode (Hamamatsu Photonics, G5125-10) as a probe light and a detector, respectively. Details of the transient absorption measurements were described elsewhere.[40] All the samples in a quartz cell (1 × 1 cm) were deaerated by bubbling argon through the solution for 15 min. Steady-state absorption spectra in the visible and near-IR regions were measured on a JASCO V570 DS spectrometer. Fluorescence spectra were measured on a Shimadzu RF-5300PC spectrofluorophotometer.

Electrochemical Measurements. The cyclic voltammetry measurements were performed on a BAS CV-50 W electrochemical analyzer in deaerated PhCN or DMF solution (0.5 mM) containing 0.1 M tetra-*n*-butylammonium perchlorate as a supporting electrolyte at 298 K (100 mV s^{-1}). The glassy carbon working electrode was polished with BAS polishing alumina suspension and rinsed with acetone before use. The counter electrode was a platinum wire. The measured potentials were recorded with respect to an Ag/AgCl (saturated KCl) reference electrode, and Fc/Fc^+ was used as an internal standard.

Theoretical Calculations. All calculations were performed by semiempirical PM3 and density function B3LYP/3-21G(*) method with Gaussian 98 package. The graphics of HOMO and LUMO coefficients were generated with the help of *Gauss View* software.

Acknowledgment. This work was partly supported by a Grant-in-Aid for Scientific Research on Priority Area (417) from the Ministry of Education, Science, Sports and Culture of Japan.

Supporting Information Available: Optimized structures for the PICT and TICT of C_{60}−PBTDP−TPA and cyclic voltammograms of C_{60}−PBTDP−TPA in PhCN. UV/vis spectra

and time-resolved fluorescence spectra of PBTDP−TPA. Nanosecond transient absorption spectra of C_{60}−PBTDP−TPA. This material is available free of charge via the Internet at http://pubs.acs.org.

References and Notes

(1) Foote, C. S. In *Topics in Current Chemistry; Photophysical and Photochemical Properties of Fullerenes*; Matty, J., Ed.; Series 169; Springer-Verlag: Berlin, 1994; p p347.

(2) *Fullerene, Chemistry, Physics and Technology*; Kadish, K. M., Ruoff, R. S., Eds.; Wiley-Interscience: New York, 2000.

(3) *Molecular and Supramolecular Photochemistry*; Ramamurthy, V., Schanze, K. S., Eds.; Marcel Dekker: New York, 2001; Vol. 7.

(4) (a) Imahori, H.; Sakata, Y. *Adv. Mater.* **1997**, *9*, 537. (b) Martín, N.; Sánchez, L.; Illescas, B.; Pérez, I. *Chem. Rev.* **1998**, *98*, 2527. (c) Guldi; D. M.; Prato, M. *Acc. Chem. Res.* **2000**, *33*, 695.

(5) Echegoyen, L.; Echegoyen, L. E. *Acc. Chem. Res.* **1998**, *31*, 593.

(6) Gust, D.; Moore, T. A.; Moore, A. L. *Acc. Chem. Rec.* **2001**, *34*, 40.

(7) (a) Williams, R. M.; Zwier, J. M.; Verhoeven, J. W. *J. Am. Chem. Soc.* **1995**, *117*, 4093. (b) Williams, R. M.; Koeberg, M.; Lawson, J. M.; An, Y.-Z.; Rubin, Y.; Paddon-Row: M. N.; Verhoeven, *J. Org. Chem.* **1996**, *61*, 5055. (c) Thomas, K. G.; Biju, V.; George, M. V.; Guldi, D. M.; Kamat, P. V. *J. Phys. Chem. A* **1998**, *102*, 5341. (d) Thomas, K. G.; Biju, V.; Guldi, D. M.; Kamat, P. V.; George, M. V. *J. Phys. Chem. B* **1999**, *103*, 8864. (e) Thomas, K. G.; Biju, V.; Guldi, D. M.; Kamat, P. V.; George, M. V. *J. Phys. Chem. A* **1999**, *103*, 10755. (f) Komamine, S.; Fujitsuka, M.; Ito, O.; Moriwaki, K.; Miyata, T.; Ohno, T. *J. Phys. Chem. A* **2000**, *104*, 11497.

(8) (a) Liddell, P. A.; Kuciauskas, D.; Sumida, J. P.; Nash, B.; Nguyen, D.; Moore, A. L.; Moore, T. A.; Gust, D. *J. Am. Chem. Soc.* **1997**, *119*, 1400. (b) Imahori, H.; Yamada, K.; Hasegawa, M.; Taniguchi, S.; Okada, T.; Sakata, Y. *Angew. Chem., Int. Ed. Engl.* **1997**, *36*, 2626. (c) Luo, C.; Guldi, D. M.; Imahori, H.; Tamaki, K.; Sakata, Y. *J. Am. Chem. Soc.* **2000**, *122*, 6535. (c) Imahori, H.; Guldi, D. M.; Tamaki, K.; Yoshida, Y.; Luo, C.; Sakata, Y.; Fukuzumi, S. *J. Am. Chem. Soc.* **2001**, *123*, 6617. (d) Imahori, H.; Tamaki, K.; Araki, Y.; Sekiguchi, Y.; Ito, O.; Sakata, Y.; Fukuzumi, S. *J. Am. Chem. Soc.* **2002,** *124*, 5165. (e) Liddell, P. A.; Kodis, G.; Moore, A. L.; Moore, T. A.; Gust, D. *J. Am. Chem. Soc.* **2002,** *124*, 7668.

(9) (a) Linssen, T. G.; Durr, K.; Hannack, M.; Hirsh, A. *J. Chem. Soc., Chem. Commun* **1995**, 103. (b) Durr, K.; Fiedler, S.; Linssen, T.; Hirshi, A.; Hanack; M. *Chem. Ber.* **1997**, *130*, 1375. (c) Saster, A.; Gouloumis, A.; Vazques, P.; Torres, T.; Doan, V.; Schwartz, B. J.; Wudl, F.; Echigoyen, L.; Rivera, J. *Org. Lett.* **1999**, *1*, 1807. (d) Martinez-Diaz, M. V.; Fender, N. S.; Rodriguez-Morgade, M. S.; Gomes-Lopes, M.; Dietrich, F.; Echioyen, L.; Stoddart, J. F.; Torres, T. J. *Mater. Chem.* **2002**, *12*, 2095. (e) Guldi, D. M.; Ramey, J.; Martinez-Diaz, M. V.; de la Escosura, A.; Torres, T.; Da Ros, T.; Prato, M. *Chem. Commun.* **2002**, 2774.

(10) (a) Sacricifici, N. S.; Wudl, F.; Heeger, A. J.; Maggini, M.; Scorrano, G.; Prato, M. Bourassa, J.; Ford, P. C. *Chem. Phys. Lett.* **1995**, *247*, 210. (b) Maggini, M.; Guldi, D. M.; Mondini, S,; Scorrano, G.; Paolucci, F.; Ceroni, P.; Roffia, S. *Chem. Eur. J.* **1998**, *4*, 1992. (c) Maggini, M,; Dono, A.; Scorrano, G.; Prato, M. *J. Chem. Soc., Chem. Commun.* **1998**, 845.

(11) (a) Guldi, D. M.; Maggini, M.; Scorrano, G.; Prato, M. *J. Am. Chem. Soc.* **1997**, *119*, 974. (b) D'Souza, F.; Zandler, M. E.; Smith, P. M.; Deviprasad, G. R.; Arkady, K.; Fujitsuka, M.; Ito, O. *J. Phys. Chem. A* **2002**, *106*, 649. (c) Zandler, M. E.; Smith, P. M.; Fujitsuka, M.; Ito, O.; D'Souza, F. *J. Org. Chem.*, **2002**, *67*, 9122. (d) Fujitsuka, N. Tsuboya, R. Hamasaki, M. Ito, S. Onodera, S.; Ito, O.; Yamamoto, Y. *J. Phys. Chem. A* **2003**, *107*, 1452.

(12) (a) Martín, N.; Sánchez, L.; Herranz, M. A. Guldi, D. M. *J. Phys. Chem. A* **2000**, *104*, 4648. (b) Herranz, M. A.; Ollescas, B., Martín, N.; Luo, C.; Guldi, D. M. *J. Org. Chem.* **2000**, *65*, 5728. (c) Martín, N.; Sánchez, L.; Guldi, D. M. *Chem. Commun.* **2000**, 113. (d) Martín, N.; Sánchez, L.; Illescas, B.; González, S.; Herranz, M. A.; Guldi, D. M. *Carbon* **2000**, *38*, 1577. (e) Allard, E.; Cousseau, J.; Oruduna, J.; Garin, J.; Luo; H.; Araki, Y.; Ito, O. *Phys. Chem. Chem. Phys.* **2002**, *4*, 5944. (f) Kreher, D.; Hudhomme, P.; Gorgues, A.; Luo; H.; Araki, Y.; Ito, O. *Phys. Chem. Chem. Phys.* **2003**, *5*, 4583. (g) Sánchez, L.; Pérez, I.; Martín, N.; Guldi, D. M. *Chem. Eur. J.* **2003**, *9*, 2457.

(13) (a) Yamashiro, T.; Aso, Y.; Otsubo, T.; Tang, H.; Harima, T.; Yamashita, K. *Chem. Lett.* **1999**, 443. (b) Fujitsuka, M.; Ito, O.; Yamashiro, T.; Aso, Y.; Otsubo, T. *J. Phys. Chem. A* **2000**, *104*, 4876. (c) Hirayama, D.; Yamashiro, T.; Takiyama, K.; Aso, Y.; Otsubo, T.; Norieda, H.; Imahori, H.; Sakata, Y. *Chem. Lett.* **2000**, 570. (d) van Hal, P. A.; Knol, J.; Langeveld-Voss, B. M. W.; Meskers, S. C. J.; Hummelen, J. C.; Janssen, R. A. J. *J. Phys. Chem. A* **2000**, *104*, 5974.

(14) (a) Fujitsuka, M.; Matsumoto, K.; Ito, O.; Yamashiro, T.; Aso, Y.; Otsubo, T. *Res. Chem. Intermed.* **2001**, *27*, 73. (b) van Hal, P. A.; Beckers, E. H. A.; Meskers, S. C. J.; Janssen, R. A. J.; Jousselme, B.; Blanchard, P.; Roncali, J. *Chem. Eur. J.* **2002**, *8*, 5415. (c) Beckers, E. H. A.; van Hal, P. A.; Dhanabalan, A.; Meskers, S. C. J.; Knol, J.; Hummelen, J. C.; Janssen, R. A. J. *J. Phys. Chem. A* **2003**, *107*, 6218.

(15) Luo, H.; Fujitsuka, M.; Araki, Y.; Ito, O.; Padmawar, P.; Chiang, L. Y. *J. Phys. Chem. B* **2003**, *107*, 9312.

(16) (a) Imahori, H.; Hagiwara, K.; Akiyama, T.; Akoi, M.; Taniguchi, S.; Okada, T.; Shirakawa, M.; Sakata, Y. *Chem. Phys. Lett.* **1996**, *263*, 545. (b) Guldi, D. M.; Asmus, K.-D. *J. Am. Chem. Soc.* **1997**, *119*, 5744. (c) Imahori, H.; El-Khouly, M. E.; Fujitsuka, M.; Ito, O.; Sakata, Y.; Fukuzumi, S. *J. Phys. Chem. A.* **2001**, *105*, 325. (d) Imahori, H.; Tamaki, K.; Guldi, D. M.; Luo, C.: Fujitsuka, M.; Ito, O.; Sakata, Y.; Fukuzumi, S. *J. Am. Chem. Soc.* **2001**, *123*, 2607. (e) Vehmanen, V.; Tkachenko, N. V.; Imahori, H.; Fukuzumi, S.; Lemmetyinen, H. *Spectrochim. Acta, Part A* **2001**, *57*, 2229.

(17) (a) *The Photosynthetic Reaction Center*; Deisenhofer, J., Norris, J. R., Eds.; Academic Press: San Diego, 1993. (b) *Anoxygenic Photosynthetic Bacteria*; Blankenship, R. E., Madigan, M. T., Bauer, C. E., Eds.; Kluwer Academic Publishing: Dordrecht, 1995. (c) Wasielewski, M. R.; Wiederrecht, G. P.; Svec, W. A.; Niemczyk, M. P. *Sol. Energy Mater. Solar Cells* **1995**, *38*, 127.

(18) (a) Imahori, H.; Cardoso, S.; Tatman, D.; Lin, S.; Noss, L.; Seely, G. R.; Sereno, L.; Silber, C.; Moore, T. A.; Moore, A. L.; Gust, D. *Photochem. Photobiol.* **1995**, *62*, 1009. (b) Gust, D.; Moore, T. A.; Moore, A. L.; *Res. Chem. Interned.* **1997**, *23*, 621. (c) Yamazaki, M.; Araki, Y.; Fujitsuka, M.; Ito, O. *J. Phys. Chem. A* **2001**, *105*, 8615. (d) González, S.; Herranz, M. A.; Illescas, B.; Segura, J. L.; Martín, N. *Synth. Met.* **2001**, *121*, 1131.

(19) Yamanaka, K.; Fujitsuka, M.; Araki, Y.; Ito, O.; Aoshima, T.; Fukushima, T.; Miyashi, T. *J. Phys. Chem. A*, **2004**, *108*, 250.

(20) Bell, T. D. M.; Smith, T. A.; Ghiggino, K. P.; Ranasinghe, M. G.; Shephard, M. J.; Paddon-Row, M. *Chem. Phys. Lett.* **1997**, *268*, 223−228.

(21) (a) Raimundo, J.-M.; Blanchard, P.; Brisset, H.; Akoudad, S.; Roncali, J. *Chem. Commun.* **2000**, 939. (b) Akhtaruzzaman, M.; Tomura, M.; Zaman, M. B.; Nishida, J.; Yamashita, Y. *J. Org. Chem.* **2002**, *67*, 7813. (c) Edelmann, M. J.; Raimundo, J.-M.; Utesch, N. F.; Diederich, F.; Boudon, C.; Gisselbrecht, J.-P.; Gross, M. *Helv. Chim. Acta* **2002**, *85*, 2195.

(22) (a) Kitamura, C.; Tanaka, S.; Yamashita, Y. *Chem. Mater.* **1996**, *8*, 570. (b) van Mullekom, H. A. M.; Vekemans, J. A. J. M.; Meijer, E. W. *Chem. Eur. J.* **1998**, *4*, 1235. (c) Bangcuyo, C. G.; Evans, U.; Myrick, M. L.; Bunz, U. H. F. *Macromolecules* **2001**, *34*, 7592. (d) Niu, Y.-H.; Huang, J.; Cao, Y. *Adv. Mater.* **2003**, *15*, 807.

(23) Zhang, X.; Gorohmaru, H.; Kadowaki, M.; Kobayashi, T.; Ishi-i, T.; Thiemann, T.; Mataka, S. *J. Mater. Chem.* **2004**, *14*, 1901.

(24) Kato, S.; Matsumoto, T.; Ishi-i, T.; Thiemann, T.; Shigeiwa, M.; Gorohmaru, H.; Maeda, S.; Yamashita, Y.; Mataka, S. *Chem. Commun.* **2005**, 2342.

(25) (a) Rettig, W. *Angew. Chem., Int. Ed. Engl.* **1986**, *25*, 969. (b) Rettig, W. *Top. Curr. Chem.* **1994**, *169*, 253. (c) Rettig, W.; Lapouyade, R. *Top. Fluoresc. Spectrosc.* **1994**, *4*, 109.

(26) Wang, X.; Perzon, E.; Delgado, J. L.; de la Cruz, P.; Zhang, F.; Langa, F.; Andersson, M.; Inganas, O. *Appl. Phys. Lett.* **2004**, *85*, 5081.

(27) Sandanayaka, S. D. A.; Matsukawa, K.; Ishi-i, T.; Mataka, S.; Araki, Y.; Ito, O. *J. Phys. Chem. B* **2004**, *108*, 19995.

(28) (a) Maggini, M.; Scorrano, G.; Prato, M. *J. Am. Chem. Soc.* **1993**, *115*, 9798. (b) Prato, M.; Maggini, M. *Acc. Chem. Res.* **1998**, *31*, 519. (c) Prato, M.; Maggini, M.; Giacometti, C.; Scorrano, G.; Sandonà, G.; Farnia, G. *Tetrahedron* **1996**, *52*, 5221.

(29) Weller, A. *Z. Phys. Chem. Neue Folge* **1982**, *133*, 93.

(30) The energy levels of the lowest singlet excited states of PBTDP−TPA were evaluated from the fluorescence peaks, because it was difficult to evaluate the 0−0 transition due to large Stokes shift.

(31) (a) Arbogast, J. W.; Foote, C. S.; Kao, M. *J. Am. Chem. Soc.* **1992**, *114*, 2277. (b) Biczok, L.; Linschitz, H. *Chem. Phys. Lett.* **1992**, *195*, 339. (c) Nonell, S.; Arbogast, J. W.; Foote, C. S. *J. Phys. Chem.* **1992**, *96*, 4169. (d) Steren, C. A.; von Willigen, H.; Biczok, L.; Gupta, N.; Linschitz, H. *J. Phys. Chem.* **1996**, *100*, 8920. (e) Luo, C.; Fujitsuka, M.; Watanabe, A.; Ito, O.; Gan, L.; Huang, Y. Huang, C.-H. *J. Chem. Soc., Faraday Trans.* **1998**, *94*, 527.

(32) (a) Sension, R. J.; Phillips, C. M.; Szarka, A. Z.; Romanow, W. J.; McGhie, A. R.; McCauly, J. P., Jr.; Smith, A. B., III; Hochstrasser, R. M. *J. Phys. Chem.* **1991**, *95*, 6075. (b) Ebbesen, T. W.; Tanigaki, K.; Kuroshima, S. *Chem. Phys. Lett.* **1991**, *181*, 501. (c) Lee, M.; Song, O.-K.; Seo, J.-C.; Kim, D.; Suh, Y. D.; Jin, S. M.; Kim, S. K. *Chem. Phys. Lett.* **1992**, *196*, 325. (d) Watanabe, A.; Ito, O.; Watanabe, M.; Saito, H.; Koishi, M. *J. Chem. Soc., Chem. Commun.* **1996**, 117.

(33) (a) Lippert, E. Z. *Elektrochem.* **1957**, *61*, 962. (b) Mataga, N.; Kaifu, Y.; Koizumi, M. *Bull. Chem. Soc. Jpn.* **1956**, *29*, 465.

(34) (a) Yonemura, H.; Moribe, S.; Hayashi, K.; Noda, M.; Tokudome, H.; Yamada, S.; Nakamura, H. *Appl. Magn. Reson.* **2003**, *23*, 289. (b) Galili,

T.; Regev, A.; Levanon, H.; Schuster, D. I.; Guldi, D. M. *J. Phys. Chem. A.* **2004**, *108*, 10632.

(35) Sandanayaka, S. D. A.; Sasabe, H.; Araki, Y.; Furusho, Y.; Ito, O.; Takata, T. *J. Phys. Chem. A* **2004**, *108*, 5145.

(36) (a) Marcus, R. A. *J. Chem. Phys.* **1956,** *24*, 966. (b) Marcus, R. A. *J. Chem. Phys.* **1957,** *26*, 867. (c) Marcus, R. A. *J. Chem. Phys.* **1957,** *26*, 872. (d) Marcus, R. A. *J. Chem. Phys.* **1965,** *43*, 679. (e) Marcus, R. A.; Sutin, N. *Biochim. Biophys. Acta* **1985,** *811*, 265.

(37) (a) Ohkubo, K.; Imahori, H.; Shao, J.; Ou, Z.; Kadesh, K. M.; Chen, Y.; Zheng, G.; Pandey, R. K.; Fujitsuka, M.; Ito, O.; Fukuzumi, S. *J. Phys. Chem. A* **2002**, *106*, 10991. (b) Ohkubo, K.; Kotani, H.; Shao, J.; Ou, Z.; Kadesh, K. M.; Li, G.; Pandey, R. K.; Fujitsuka, M.; Ito, O.; Imahori, H.; Fukuzumi, S. *Angew. Chem., Int. Ed.* **2004**, *43*, 853.

(38) Pilgram, K.; Zupan, M.; Skiles, R. *J. Heterocycl. Chem.* **1970**, *7*, 629.

(39) (a) Watanabe, N.; Kihara, N.; Furusho, Y.; Takata, T.; Araki, Y. Ito, O. *Angew. Chem., Int. Ed.* **2003**, *42*, 681. (b) Choi, M. S.; Aida, T.; Luo, H.; Y. Araki, Y.; Ito, O. *Angew. Chem., Int. Ed.* **2003**, *42*, 4060. (c) Nishikawa, H.; Kojima, S.; Kodama, T.; Ikemoto, I.; Suzuki, S.; Kikuchi, K. Fujitsuka, M. Luo, H.; Araki, Y.; Ito, O. *J. Phys. Chem. A* **2004**, *108*, 1881. (d) Makinoshima, T.; Fujitsuka, M.; Sasaki, M.; Araki, Y.; Ito, O.; Ito, S.; Morita, N. *J. Phys. Chem. A* **2004**, *108*, 368.

(40) (a) Ito, O.; Sasaki, Y.; Yoshikawa, Y.; Watanabe. A. *J. Phys. Chem*. **1995**, 99, 9838. (b) Ito, O.; *Res. Chem. Intermed*. **1997**, *23*, 389. (c) Yahata, Y.; Sasaki, Y.; Fujitsuka, M.; Ito, O. *J. Photosci.* **1999**, *6*, 117.